Tracking the Evolution of Lithium in Giants Using Asteroseismology: Super-Li-rich Stars Are Almost Exclusively Young Red-clump Stars

Raghubar Singh[1,2] ✆, Bacham E. Reddy[1], Simon W. Campbell[3], Yerra Bharat Kumar[4,6], and Mathieu Vrard[5]

[1] Indian Institute of Astrophysics, 560034, 100ft Road Koramangala, Bangalore, India; raghubar2015@gmail.com
[2] Pondicherry University R.V. Nagara, Kala Pet, 605014, Puducherry, India
[3] School of Physics and Astronomy, Monash University, Clayton, Victoria, Australia
[4] Key Laboratory for Optical Astronomy, National Astronomical Observatories, Chinese Academy of Sciences, Beijing, 100101, People's Republic of China
[5] Dept. of Astronomy, The Ohio State University, 140 W. 18th Avenue, Columbus, OH 43210, USA

Abstract

We report novel observational evidence on the evolutionary status of lithium-rich giant stars by combining asteroseismic and lithium abundance data. Comparing observations and models of the asteroseismic gravity-mode period spacing $\Delta\Pi_1$, we find that super-Li-rich giants (SLRs, $A(\text{Li}) > 3.2$ dex) are almost exclusively young red-clump (RC) stars. Depending on the exact phase of evolution, which requires more data to refine, SLR stars are either (i) less than ~ 2 Myr or (ii) less than ~ 40 Myr past the main core helium flash (CHeF). Our observations set a strong upper limit for the time of the inferred Li-enrichment phase of <40 Myr post-CHeF, lending support to the idea that lithium is produced around the time of the CHeF. In contrast, the more evolved RC stars (>40 Myr post-CHeF) generally have low lithium abundances ($A(\text{Li}) < 1.0$ dex). Between the young, super-Li-rich phase, and the mostly old, Li-poor RC phase, there is an average reduction of lithium by about 3 orders of magnitude. This Li destruction may occur rapidly. We find the situation to be less clear with stars having Li abundances between the two extremes of super-Li-rich and Li-poor. This group, the "Li-rich" stars ($3.2 > A(\text{Li}) > 1.0$ dex), shows a wide range of evolutionary states.

1. Introduction

The origin of strong lithium abundance excess in red giants —"Li-rich giants"—has been a long-standing problem ever since its discovery about four decades ago (Wallerstein & Sneden 1982). In the last few years significant progress has been made thanks primarily to large data sets of ground-based spectroscopic surveys such as LAMOST (Cui et al. 2012) and GALAH (De Silva et al. 2015), and the space-based Gaia astrometric (Gaia Collaboration et al. 2016, 2018) and Kepler time-resolved photometric surveys (Borucki et al. 2010). Studies using data from these surveys have now confirmed the early suspicions (e.g., Kumar et al. 2011; Silva Aguirre et al. 2014) that Li-rich giants are predominantly in the He-core burning phase of stellar evolution, also known as the red clump (RC; Bharat Kumar et al. 2018; Smiljanic et al. 2018; Casey et al. 2019; Deepak & Reddy 2019; Singh et al. 2019). This new development has significantly narrowed the search for finding the origin of the lithium enhancement.

It is also well established that Li is almost totally destroyed during the phase of evolution just preceding the RC, the red giant branch (RGB; Lind et al. 2009; Kumar et al. 2020), reaching values as low as $A(\text{Li}) \sim -1.0$ dex. In contrast, the average Li abundance on the RC is $A(\text{Li}) = +0.7$ dex (Kumar et al. 2020), implying that there must be a lithium production phase between the late RGB and RC. Since that study two theoretical models have been put forward for Li production. The first is by Mori et al. (2021) whose model produces Li at the RGB tip, before the onset of He-flash, via the inclusion of the neutrino magnetic moment. The second proposed model produces Li during the main CHeF, by assuming some ad hoc mixing during the extremely energetic flash (Schwab 2020). Both the models explain the observations,

with average RC $A(\text{Li})$ of $+0.7$ dex; however, they do not attempt to explain the (super-)Li-rich giants. That said, variation in the parameters of the Schwab (2020) model can indeed produce the very high Li abundances required (see their Figure 4), although the author notes that these high Li abundances are quickly depleted in their model. The current study attempts to better isolate the location of the Li production site as stars transition from the RGB tip to the RC phase. We also aim to explore Li evolution along the RC.

We do this by using observations of the asteroseismic parameter $\Delta\Pi_1$, the asymptotic gravity-mode period spacing of dipole modes (Unno et al. 1989; Mosser et al. 2012a, 2014; Vrard et al. 2016), which has been shown to clearly vary with evolution in stellar models of the RC phase (Bildsten et al. 2012; Bossini et al. 2015; Constantino et al. 2015). We combine $\Delta\Pi_1$ with newly derived Li abundances as well as Li abundances from the literature.

2. Sample Selection

We extracted a sample of 6955 low-mass ($M \leqslant 2\,M_\odot$) giants that are classified as RC stars based on Kepler asteroseismic data (Yu et al. 2018). We then searched the literature for $\Delta\Pi_1$ values (Mosser et al. 2012a, 2014; Vrard et al. 2016) and Li abundances (Takeda & Tajitsu 2017; Bharat Kumar et al. 2018; Singh et al. 2019; Yan et al. 2021). We found 37 stars with $A(\text{Li})$ and $\Delta\Pi_1$, and we measured $\Delta\Pi_1$ in 10 more (Section 3.2), giving a total of 47 RC stars with both parameters.

We also searched for Kepler field stars in the recently released catalog of medium-resolution (MRS, $R \approx 7500$) spectroscopic data of the LAMOST[7] survey (Liu et al. 2020), finding 577 RC
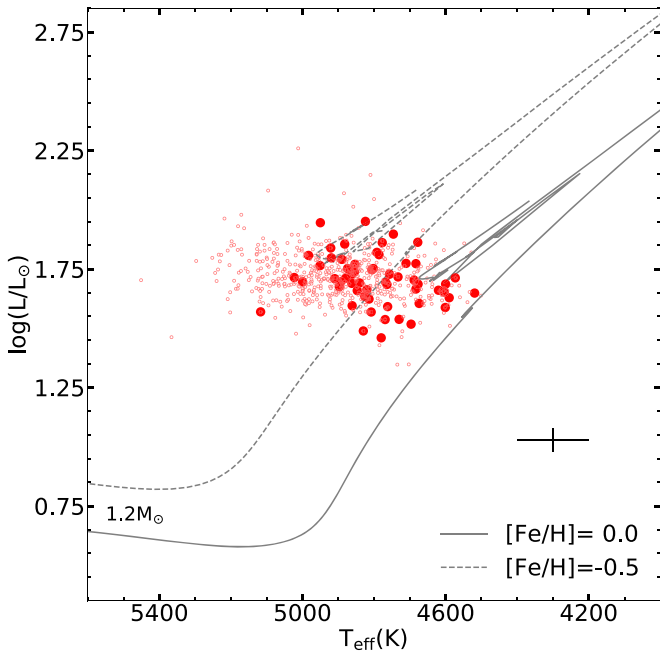
---

[6] LAMOST Fellow.

[7] http://dr6.lamost.org/

Figure 1. H-R diagram showing the sample of 59 RC giants for which we have $\Delta\Pi_1$ and A(Li) (large symbols). For context we show the entire Kepler–LAMOST-MRS overlap RC sample of 577 giants in the background. Overplotted are two stellar model tracks, both 1.2 $M_\odot$ but with two different metallicities. Typical observational uncertainties are indicated by the error cross.
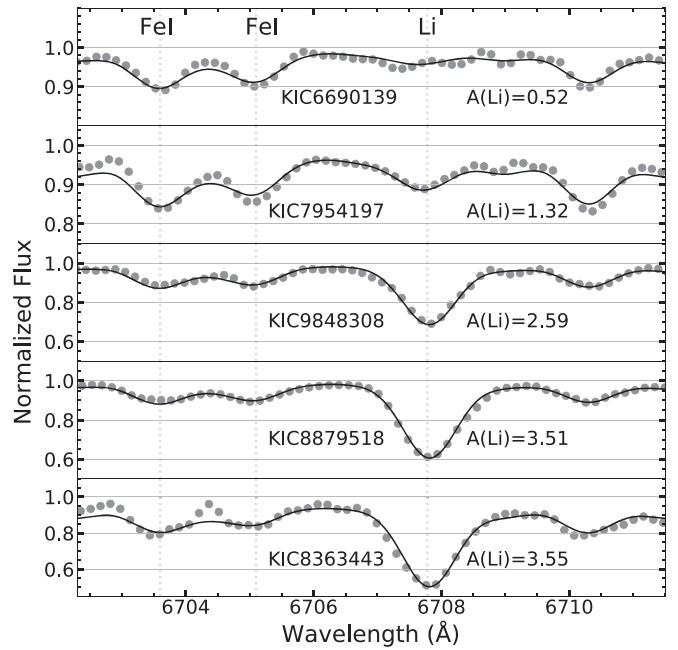

Figure 2. Derivation of Li abundances for a few representative giants using spectral synthesis of the 6707.78 Å Li line (solid lines) in the LAMOST medium-resolution spectra (dots).

stars. We were able to measure Li in 22 of these stars (Section 3.1). Of these, we found $\Delta\Pi_1$ for 6 of them in the literature (Mosser et al. 2012a, 2014; Vrard et al. 2016) and were able to measure $\Delta\Pi_1$ for a further 6 of them (Section 3.2), giving an extra 12 stars with both parameters.

Combining this sample with the literature sample, we have a total of 59 RC stars with certain evolutionary phase and accurate Li abundances, all from the Kepler field. Luminosities were derived using the Gaia distances (Gaia Collaboration et al. 2018) and the bolometric correction from Torres (2010). We discuss possible biases in our sample in the Appendix. We found no bias in our sample that could alter our conclusions. The final sample is shown in Figure 1.

3. Results

3.1. LAMOST-MRS Lithium Abundances

Li abundances were derived by matching the synthetic spectra with the the observed Li line at 6707.78 Å in the medium-resolution LAMOST spectra. We used the 2013 version of the local thermal equilibrium (LTE) radiative transfer code MOOG (Sneden 1973), in combination with the Kurucz ATLAS atmospheric models (Castelli & Kurucz 2003). Atmospheric parameters (T_{eff}, log g, [Fe/H]) were taken from the Yu et al. (2018) catalog. Our line list, with atomic and molecular data, was compiled using the Linemake code.[8] Figure 2 shows a comparison of synthetic spectra with the observed spectra of a few representative stars. The estimated uncertainty in Li abundance is the quadratic sum of uncertainties in Li abundance caused by the estimated uncertainties in atmospheric parameters for each individual star (see Table 1). Li abundances were corrected for non-LTE effects using the Δ_{NLTE} values provided by Lind et al. (2009).

We estimated the lower detectability limit in equivalent width (EW) for our data using the Cayrel (1988) formulation for uncertainties in EW for a range of signal-to-noise ratio (S/N) = 55–150. To err on the conservative side, we adopted a lower limit of $3 \times \delta$EW = (10.6–28.2) mÅ, which translates to lower limit abundances in the range +0.7 to +1.1 dex, depending on stellar parameters (Figure 2). This criterion resulted in 22 RC stars for which we could reliably derive Li abundances, for 12 of which we have $\Delta\Pi_1$ (Table 1).

3.2. Asymptotic Gravity-mode Period Spacing $\Delta\Pi_1$

Of the 59 RC giants in our sample, $\Delta\Pi_1$ values for 43 are available in the literature (Mosser et al. 2012a, 2014; Vrard et al. 2016). For the other 16 we derived it ourselves. We downloaded the time series data from the Kepler archive and converted them to the frequency domain using the Lightkurve package[9] (Lightkurve Collaboration et al. 2018). Details of our method of $\Delta\Pi_1$ estimation are given in Mosser et al. (2014) and Vrard et al. (2016). We were able to derive asymptotic values (Table 1) for 16 RC giants that have sufficient S/N in their power density spectra.

3.3. A(Li) versus $\Delta\Pi_1$: Evolution of Li along the RC

In Figure 3 we display A(Li) versus $\Delta\Pi_1$ for the RC stars. We divide the sample into three groups depending on their Li abundance:

1. Li-normal (LN): A(Li) < 1.0 dex
2. Li-rich (LR): $1.0 < A$(Li) < 3.2 dex
3. Super-Li-rich (SLR): A(Li) > 3.2 dex

The A(Li) = 1.0 dex delineation is based on the Kumar et al. (2020) study's distribution on the RC (peaked at +0.7 dex), while the A(Li) = 3.2 dex delineation is based on the interstellar medium

---

Table 1
RC Sample of 22 Stars (Out of Total 59) for Which A(Li) and/or $\Delta\Pi$ Are Measured in This Work (See Section 2 for Details)

KIC	V[a]	$T_{\rm eff}$	log g	[Fe/H]	log($L/L_\odot$)	A(Li)$_{\rm NLTE}$	$M(M_\odot)$	$\Delta\Pi_1$
			Sample from this work of LAMOST-MRS and Kepler Field					
5079905	12.56	4769 ± 139	2.38 ± 0.01	0.03 ± 0.30	1.54 ± 0.04	2.66 ± 0.21 (1)	0.92 ± 0.09	298 ± 20 (1)
6593240	11.11	4808 ± 80	2.41 ± 0.01	0.0 ± 0.15	1.57 ± 0.03	2.74 ± 0.15 (1)	0.83 ± 0.09	277 ± 20 (2)
7020392	12.40	4893 ± 100	2.39 ± 0.01	−0.25 ± 0.15	1.83 ± 0.04	1.45 ± 0.16 (1)	0.97 ± 0.12	299 ± 20 (1)
7595155	12.12	4601 ± 100	2.36 ± 0.01	0.30 ± 0.30	1.74 ± 0.03	1.23 ± 0.20 (1)	0.86 ± 0.08	291 ± 17 (2)
7612438	12.88	4921 ± 80	2.54 ± 0.01	0.07 ± 0.15	1.96 ± 0.08	1.86 ± 0.15 (1)	1.87 ± 0.10	279 ± 32 (1)
7954197	10.90	4814 ± 139	2.42 ± 0.01	0.12 ± 0.30	1.62 ± 0.03	1.32 ± 0.20 (1)	1.23 ± 0.12	269 ± 2 (1)
8363443	10.88	4606 ± 80	2.41 ± 0.01	0.38 ± 0.15	1.81 ± 0.03	3.55 ± 0.12 (1)	1.33 ± 0.09	248 ± 2 (1)
8619916	12.90	5117 ± 160	2.44 ± 0.01	−0.05 ± 0.30	1.71 ± 0.06	2.71 ± 0.25 (1)	1.11 ± 0.11	300 ± 3 (2)
8879518	11.22	4863 ± 80	2.57 ± 0.01	0.14 ± 0.15	1.73 ± 0.03	3.51 ± 0.12 (1)	1.76 ± 0.13	268 ± 3 (2)
9848308	12.28	4733 ± 80	2.49 ± 0.01	0.06 ± 0.15	1.72 ± 0.04	2.59 ± 0.12 (1)	1.36 ± 0.09	329 ± 4 (2)
9907856	12.45	4855 ± 80	2.41 ± 0.01	−0.17 ± 0.15	1.73 ± 0.01	2.56 ± 0.13 (1)	1.16 ± 0.25	328 ± 3 (2)
11129153	12.09	4830 ± 100	2.37 ± 0.03	−0.37 ± 0.15	1.63 ± 0.08	1.45 ± 0.16 (1)	1.12 ± 0.21	228 ± 11 (1)
			Sample from literature for which $\Delta\Pi_1$ values are derived in this study					
3751167	13.74	4914 ± 80	2.33 ± 0.03	−0.76 ± 0.15	1.86 ± 0.06	4.0 ± 0.35 (3)	0.95 ± 0.22	260.0 ± 13 (1)
7131376	13.99	4833 ± 152	2.45 ± 0.01	0.04 ± 0.30	1.52 ± 0.06	3.80 ± 0.35 (3)	1.25 ± 0.11	250.8 ± 18 (1)
7899597	13.61	4757 ± 80	2.40 ± 0.03	−0.10 ± 0.15	1.77 ± 0.05	3.39 ± 0.06 (4)	1.28 ± 0.23	267.4 ± 18 (1)
8869656	9.34	4915 ± 137	2.40 ± 0.01	−0.13 ± 0.30	1.68 ± 0.02	3.61 ± 0.09 (4)	1.21 ± 0.13	235.5 ± 13 (1)
9667064	13.35	4802 ± 80	2.38 ± 0.03	0.04 ± 0.15	1.86 ± 0.06	4.40 ± 0.35 (3)	1.40 ± 0.20	260.9 ± 16 (1)
9833651	12.52	4730 ± 80	2.49 ± 0.01	0.14 ± 0.15	1.66 ± 0.04	3.40 ± 0.09 (4)	1.50 ± 0.13	266.4 ± 3 (1)
11615224	11.15	4888 ± 100	2.38 ± 0.01	−0.03 ± 0.15	1.89 ± 0.05	2.84 ± 0.02 (4)	0.85 ± 0.10	257.7 ± 2 (1)
11658789	13.35	5226 ± 155	2.42 ± 0.02	−0.52 ± 0.30	1.69 ± 0.03	3.90 ± 0.35 (3)	0.87 ± 0.14	256.0 ± 2 (1)
11805390	9.78	4950 ± 80	2.58 ± 0.01	−0.06 ± 0.15	1.65 ± 0.03	2.24 ± 0.10 (4)	1.34 ± 0.10	247.9 ± 2 (1)
12784683	11.46	4983 ± 145	2.37 ± 0.02	−0.30 ± 0.30	1.68 ± 0.02	2.79 ± 0.08 (4)	1.16 ± 0.18	282.3 ± 18 (1)

Note. Masses were derived using the relation given in Kjeldsen & Bedding (1995).
[a] https://simbad.u-strasbg.fr/simbad/sim-fbasic
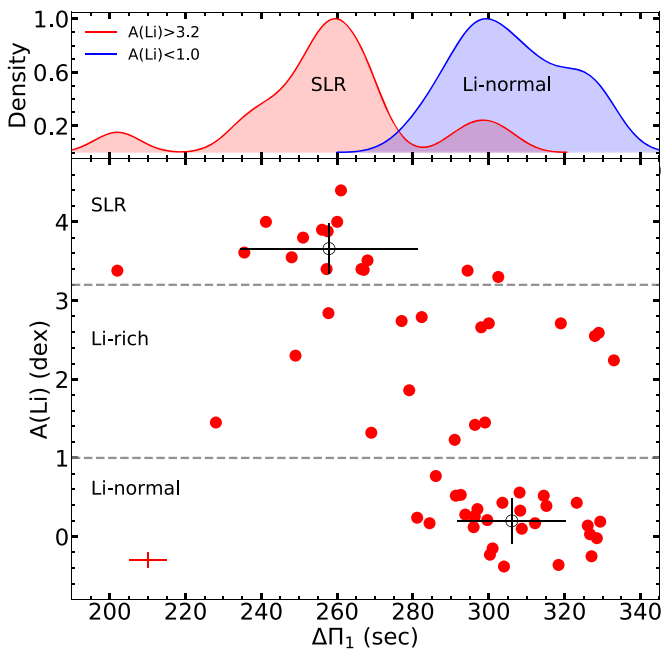**References.** (1) This work; (2) Vrard et al. (2016); (3) Singh et al. (2019); (4) Yan et al. (2021).

Figure 3. Variation of A(Li) with asymptotic gravity-mode period spacing $\Delta\Pi_1$ in RC stars. The open circles with error bars show the mean and 1σ dispersion of the groups. Due to the broadness of the Li-rich group we do not assign a mean to it. The top panel shows Gaussian kernel density histograms for the SLR and LN groups. Since $\Delta\Pi_1$ tracks the evolution of the stars (from left to right, see Figure 4), it can be seen that the average Li abundance reduces with evolution. Typical A(Li) and $\Delta\Pi_1$ uncertainties are represented by the error cross at the bottom left.

value (Knauth et al. 2003). Our key result emerges from Figure 3 —the great majority (12/15 = 80%) of the SLR stars have $\Delta\Pi_1$ peaked at low values (mean = 257 ± 23 s). We note that two of the three outliers in the SLR group have masses 2σ from the mean mass of our RC sample ($\sim$1.8 $M_\odot$, where the sample mean mass is 1.2 ± 0.3 $M_\odot$). Without these three outliers[10] the average remains the same, at 255 s, but the dispersion is halved (σ = 10 s), as expected from the histogram. In contrast, the Li-normal stars all have higher $\Delta\Pi_1$, ranging from 280 s up to $\sim$330 s. Their mean is 306 ± 14 s, much higher than the SLR group.

The Li-rich stars (Figure 3) show more complex behavior. They have a very broad distribution of $\Delta\Pi_1$ values rather than forming a coherent group. We now discuss the implications of the $\Delta\Pi_1$–A(Li) observations in relation to stellar evolution.

4. Discussion

4.1. Observations versus Stellar Evolution

Low-mass giants ($\leqslant$2 $M_\odot$) develop electron-degenerate cores while ascending the RGB. Initiation of an off-center helium flash in the degenerate core terminates the RGB evolution (Schwarzschild & Härm 1962; Demarque & Mengel 1971; Sweigart 1994). The first/main He-flash is very short-lived, lasting about 1000 yr. After the main flash a series of progressively weaker flashes ensues (Figure 4; also see Thomas 1967; Cassisi et al. 2003; Bildsten et al. 2012;

_____
[10] We do not remove these stars from the sample; this is only a test of the sensitivity of the dispersion, since with the outliers the distribution is non-Gaussian.
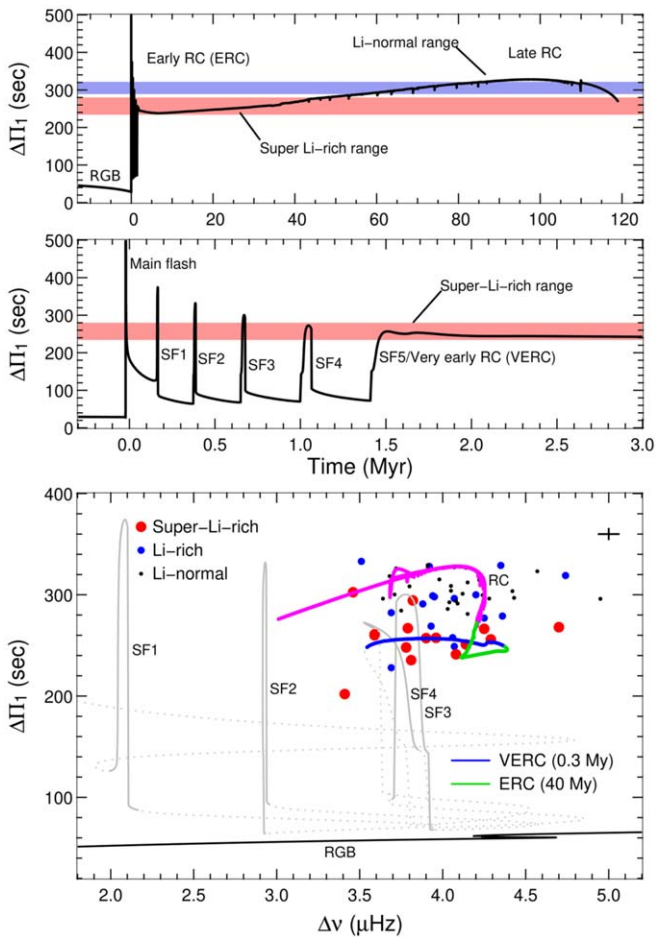
Figure 4. Stellar model showing evolution of $\Delta\Pi_1$ and $\Delta\nu$. Top panel: $\Delta\Pi_1$ evolution through the late RGB, the brief helium core flash phase, and the entire RC phase. The shaded bands show the 1σ intervals of $\Delta\Pi_1$ for the SLR (red) and Li-normal stars (blue), corresponding to the distributions in Figure 3. Middle panel: same as the top panel, but magnified to focus on the helium flashing phase and the early RC. Bottom panel: model evolution in the $\Delta\Pi_1$–$\Delta\nu$ plane (lines), compared to observations. Dotted lines are used for the evolution between (sub)flashes for clarity.

Deheuvels & Belkacem 2018), each igniting closer and closer to the center, progressively removing the electron degeneracy in the core. The entire He-flashing phase lasts $\sim$1.5–2 Myr. Finally the very center of the core becomes convective, marking the start of the RC phase (quiescent core helium burning), which lasts for $\sim$100 Myr. Throughout this evolution $\Delta\Pi_1$ varies predictably, as seen in Figure 4 (also see Bildsten et al. 2012; Constantino et al. 2015; Bossini et al. 2015; Deheuvels & Belkacem 2018). Our new observational data enable us to compare the observed $\Delta\Pi_1$ with model predictions.

We have calculated a series of stellar models using the MESA code (version 12778; Paxton et al. 2011, 2019) that vary in mass[11] ($M = 0.9$, 1.2, 1.4 $M_\odot$) and metallicity ([Fe/H] = -0.4, $+0.0$), to cover the bulk of our observational sample. RGB mass loss was modeled using the Reimers (1975) formula ($\eta = 0.3$). We used the standard MESA nuclear network ("basic.net") and standard equation of state (see Paxton et al. 2019 for details), and $\alpha_{MLT} = 2.0$. Convective boundary locations were based on the Schwarzschild criterion,

extended with exponential overshoot (Herwig et al. 1997). In Figure 4 we show a representative model that matches the mean mass of our sample, 1.2 $M_\odot$, and is of solar metallicity[12] (the mean [Fe/H] of our sample is -0.14 ± 0.26 dex). As Bossini et al. (2017) showed, the very early RC $\Delta\Pi_1$ evolution is not dependent on mass; however, it has some dependence on metallicity. Comparing the dispersion of [Fe/H] in our sample (0.26 dex) with the models in Figure 3 of Bossini et al. (2017), we expect a variation of $\sim$5 s in $\Delta\Pi_1$. This is approximately the same as our observational error bars (Figure 3). On the other hand, the late RC is particularly sensitive to the treatment of convective boundaries (e.g., Constantino et al. 2015; Bossini et al. 2015). To match the highest $\Delta\Pi_1$ values ($\sim$330 s) we adopted an overshoot parameter $f_{OS} = 0.02$.

We display the model evolution of $\Delta\Pi_1$ versus time in the top panels of Figure 4. Overplotted are the 1σ intervals of $\Delta\Pi_1$ for the observations of the SLR and Li-normal groups (see Figure 3). It can be seen that the high values of $\Delta\Pi_1$ of the Li-normal stars are only available in the second half of the RC evolution (from $\sim$40 Myr onward), or for extremely brief periods ($\sim$0.005 Myr) during the early helium flashes, which are unlikely to be observed in such numbers. We thus identify the Li-normal stars as more evolved RC stars.

In contrast, the low $\Delta\Pi_1$ values of the SLR stars are only consistent with young RC stars ($\lesssim$40 Myr in the 1.2 $M_\odot$ model). Interestingly we find there is very little overlap between the Li-normal and SLR populations. This may indicate a rapid Li-depletion event (but see Section 4.4).

4.2. Are SLR Stars He-flash Stars?

One of the main hypotheses for the Li-enrichment event is that it occurs during the main helium flash (Kumar et al. 2011; Mocák et al. 2011; Silva Aguirre et al. 2014; Kumar et al. 2020; Schwab 2020). Here we explore the possibility that our sample of SLR stars are currently experiencing the CHeF, or are in the following subflashing phases.

In Figure 4 it can be seen that there is some degeneracy in $\Delta\Pi_1$ during the early phases of the RC evolution. This makes identifying the exact young RC phase that the SLR stars reside in more difficult.

The vertical portions of the $\Delta\Pi_1$ evolution are extremely short-lived, so it is very unlikely to find stars in these phases. Adding the extra dimension of $\Delta\nu$ (bottom panel of Figure 4), we see that the $\Delta\nu$ values of the model's early subflashes are inconsistent with our sample. This is also true of the main CHeF (not pictured), which has $\Delta\nu \sim 0.04$ μHz. In addition, the main flash has $\Delta\Pi_1 = 700$ s, well outside our observed range. Thus, we can rule out our SLR stars being in the main core helium flash. The third subflash (SF3) has $\Delta\Pi_1 \sim 300$ s, well above the SLR average value of 257 s, so we rule this out also. We checked the variation of $\Delta\Pi_1$ during the subflashes in our small set of models and found only small deviations of $\sim \pm 5$ s in our mass and metallicity range.[13] This variation is similar to our uncertainties on $\Delta\Pi_1$. Three possibilities remain, defined by the SLR $\Delta\Pi_1$ band:

1. The first $\sim$40 Myr of RC evolution, "early RC" (ERC in Figure 4);

---

[11] We note that the seismic masses are the current masses of the stars. The total RGB mass loss is $\sim$0.1 $M_\odot$, which is small compared to the dispersion of our sample (0.3 $M_\odot$).

[13] The number of SFs remain the same (five), but there are some small differences in timescales, dependent on mass and metallicity. The similarity is due to the He cores all being quite similar, which also gives rise to the RC itself.

2. The first $\sim$0.3 Myr of evolution, which encompasses the "merged" subflash SF5, named "very early RC" (VERC: 1.6–1.9 Myr range in Figure 4);

3. The final separated helium subflash, SF4, which has a lifetime of 0.04 Myr and $\Delta\nu$ values within the range of our observations.

Large surveys give us statistical information on Li-rich giants that may also help in identifying the exact phase of SLR stars. Using the large samples of Kumar et al. (2020) and Singh et al. (2019) we have calculated the SLR fractions to be 0.3% and 0.5%, respectively. If we hypothesize that all stars go through an SLR phase, then we can estimate timescales of the SLR phase. The RC phase lasts for $\sim$100 Myr, implying that the SLR phase would last around 0.3–0.5 Myr. The lifetime of SF4 is only 0.04 Myr, so this is inconsistent with the timescale estimated from the surveys. Put another way, we find too many SLR stars for the SF4 scenario, by a factor of $\sim$10. Further, we estimated the probability of finding even one SF star in our sample and found an expectation of 0.02 stars. Given these various lines of evidence we conclude that our SLR stars are highly unlikely to be in a flashing phase.

4.3. How Young Are the SLR Stars?

To attempt to distinguish between the two remaining phases we turn to our series of models, to quantify the theoretical versus observational dispersion in $\Delta\Pi_1$ and $\Delta\nu$. We found that the various stellar tracks covered the whole observed wide range of $\Delta\nu$ for the SLR stars. Other uncertain model parameters, such as the convective mixing length α_{MLT}, would further increase the dispersion in $\Delta\nu$ (Constantino et al. 2015; Bossini et al. 2017). Thus, we are unable to distinguish between the VERC and ERC scenarios using $\Delta\nu$.

In contrast, as mentioned above, $\Delta\Pi_1$ does not vary much with mass in the early RC, as reported by Bossini et al. (2017). During the VERC phase (not reported by Bossini et al. 2017) we find a small dispersion in our set of models. The variation with mass is $\sim \pm 5$ s, and with metallicity $\sim \pm 10$ s, which is comparable to the observed dispersion of the SLR stars ($\sigma = 23$ s; or $\sigma = 10$ s if outliers are ignored, see Section 3). Thus, within the mass and metallicity variation of our sample, the ERC and VERC phases always present low $\Delta\Pi_1$ values, close to what we observe in the SLR stars. This reinforces the finding that these objects are all young, or very young, RC stars.

Unfortunately, due to the $\Delta\nu$ and $\Delta\Pi_1$ degeneracy we can not distinguish between these two phases. We now briefly discuss the implications of both scenarios.

In the ERC case only a small proportion, $\sim$1%, of stars would be super-Li-rich. This is a factor of 2–3 higher than the fraction found when taking into account all RC stars, consistent with the SLR stars being only found in the first $\sim$40% of the RC lifetime. In the VERC case $\sim$100% of low-mass stars would be SLR. That is, super-Li-richness would be a universal phase of low-mass stars. They would already be super-Li-rich as they start the RC, which would be consistent with the model of Schwab (2020), where the Li enrichment occurs during the main CHeF. A universal SLR phase would also resonate with the finding of Kumar et al. (2020), who report that all low-mass stars appear to go through a Li-enrichment phase, albeit to more moderate abundances—although this difference would be explained by our Li-normal group, which indicates that strong depletion occurs during the RC.

4.4. The Li-rich group

The Li-rich group (Figure 3) is more difficult to interpret, since the $\Delta\Pi_1$ distribution is so broad. We speculate that these stars could be in a phase of evolution intermediate to the SLR and Li-normal stars, currently depleting Li on their way to the late RC. This aligns with their $\Delta\Pi_1$ distribution being peaked at 290 s, which is between that of the SLR group (257 s) and the Li-normal group (306 s). If the Li-rich stars are currently undergoing Li depletion then it suggests the Li depletion is a slower process. More information is needed to disentangle the evolutionary state(s) of this group.

5. Conclusion

By combining asteroseismic and spectroscopic measurements for a sample of giant stars we discovered a correlation between A(Li) and $\Delta\Pi_1$, whereby super-Li-rich stars are almost universally young RC stars, and Li-normal stars are predominately older RC stars.

The simplest explanation for this is that (i) there is a Li-enrichment phase before the start of the RC, either near the RGB tip or during the core flashing phase, and (ii) Li is depleted during the early phases of RC evolution. The exact time of the Li depletion, which could be in the very early phases of RC evolution ($\sim$0.3% of RC lifetime) or later during the early RC (first $\sim$40% of RC evolution) is indistinguishable with our current data. If it occurs in the very early RC phase then it implies that *all* low-mass stars go through an SLR phase. If it occurs later then $\sim$1% go through an SLR phase. More data are required to separate these scenarios. Further, the relation between A(Li) and $\Delta\Pi_1$ will help to trace the transition of giants from the tip of RGB to RC phase where stars burn helium at the center quiescently.

Appendix
Possible Biases in Stellar Sample

Of our 59 RC giants 30 are taken from Takeda & Tajitsu (2017). This forms our low-Li sample of stars as their A(Li) are based on high-resolution spectra. The Takeda & Tajitsu (2017) sample, which only used brightness as a selection criterion, was itself taken from the original sample of Mosser et al. (2012a), who derived $\Delta\Pi_1$ for 95 RC stars that had long-cadence observations of the Kepler field.

At no stage did we select on the basis of $\Delta\Pi_1$. Our A(Li) values are however limited in a couple of cases. First, the abundances from the LAMOST medium-resolution spectra are
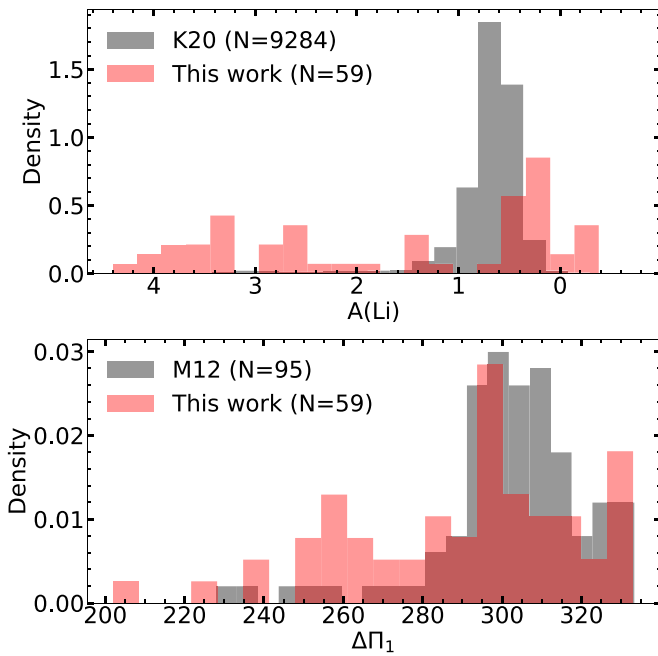
Figure 5. Histogram showing the distribution of $A(Li)$ (top) and $\Delta\Pi_1$ (bottom) of our RC sample compared to the large GALAH sample (Kumar et al. 2020, K20) and the Mosser et al. (2012a, M12) catalog. We note that at low $A(Li)$ the K20 sample has a systematic shift relative to the Takeda & Tajitsu (2017) sample, of $\sim+0.3$ dex. This could be due to the lower resolution and S/N of GALAH. The bias to high Li can be seen in our sample, as can the unusual peak in $\Delta\Pi_1$ at ~255 s associated with the SLR stars (our main result).

limited to $A(Li) \gtrsim 0.7$ dex (Section 3.1). This does not affect the detection of Li-rich and SLR stars, since their abundances are above this limit, but it biases against low-Li stars. second, we used the sample from Singh et al. (2019) whose Li measurements were restricted only to very strong Li lines due to low spectral resolution (LAMOST, $R \sim 1800$). This resulted in a bias toward SLR stars in their sample, which is mapped to our sample. By combining these samples biased to Li-rich stars with the low-Li sample of Takeda & Tajitsu (2017), we cover the whole range of $A(Li)$.

Super-Li-rich stars are central to our main result (Sections 3 and 4). The Kepler field is known to have 26 SLR stars in total (Singh et al. 2019; also Table 1); they are rare objects. Of these, we have 15 in our sample with $\Delta\Pi_1$ measurements. As such our sample represents a very substantial fraction (58%) of all the known SLR stars in the Kepler field.

A possible bias against observing low $\Delta\Pi_1$ values was reported by Constantino et al. (2015), based on comparisons between models and the Mosser et al. (2012b) sample. At low $\Delta\Pi_1$ their models predict more stars than are observed. This could be a problem with the models or the observations, or both. As mentioned, our sample contains 58% of all known Kepler field SLR stars. We have $\Delta\Pi_1$ for all of these stars, and our main result (Section 3) is that they are strongly peaked at low values. This shows that we, and others (see Section 2 for $\Delta\Pi_1$ sources), have been able to measure low values of $\Delta\Pi_1$ in the majority of these stars. We see no reason why the detectability of $\Delta\Pi_1$ should depend on Li abundance.

In Figure 5 we provide histograms comparing the distributions of $\Delta\Pi_1$ and $A(Li)$ in our sample with large survey samples. Our sample covers the whole range of $A(Li)$ and $\Delta\Pi_1$ present in the larger samples. As discussed above, our sample has proportionally more (S)LR stars than an unbiased survey, which is seen clearly in

Figure 5. The $\Delta\Pi_1$ distribution, despite being independent of our sampling, has an unusual peak at low $\Delta\Pi_1 \sim 255$ s—this is our main result, that SLR stars have predominately low $\Delta\Pi_1$.

ORCID iDs

Raghubar Singh ⓘ https://orcid.org/0000-0001-8360-9281

References

Asplund, M., Grevesse, N., Sauval, A. J., & Scott, P. 2009, ARA&A, 47, 481
Bharat Kumar, Y., Singh, R., Eswar Reddy, B., & Zhao, G. 2018, ApJL, 858, L22
Bildsten, L., Paxton, B., Moore, K., & Macias, P. J. 2012, ApJL, 744, L6
Borucki, W. J., Koch, D., Basri, G., et al. 2010, Sci, 327, 977
Bossini, D., Miglio, A., Salaris, M., et al. 2015, MNRAS, 453, 2290
Bossini, D., Miglio, A., Salaris, M., et al. 2017, MNRAS, 469, 4718
Lightkurve Collaboration, Cardoso, J. V. d. M., Hedges, C., et al. 2018, Lightkurve: Kepler and TESS time series analysis in Python, Astrophysics Source Code Library, ascl:1812.013
Casey, A. R., Ho, A. Y. Q., Ness, M., et al. 2019, ApJ, 880, 125
Cassisi, S., Schlattl, H., Salaris, M., & Weiss, A. 2003, ApJL, 582, L43
Castelli, F., & Kurucz, R. L. 2003, in IAU Symp. 210, Modelling of Stellar Atmospheres, ed. N. Piskunov, W. W. Weiss, & D. F. Gray (San Francisco, CA: ASP), A20
Cayrel, R. 1988, in IAU Symp. 132, The Impact of Very High S/N Spectroscopy on Stellar Physics, ed. G. Cayrel de Strobel & M. Spite (Dordrecht: Kluwer Academic), 345
Constantino, T., Campbell, S. W., Christensen-Dalsgaard, J., Lattanzio, J. C., & Stello, D. 2015, MNRAS, 452, 123
Cui, X.-Q., Zhao, Y.-H., Chu, Y.-Q., et al. 2012, RAA, 12, 1197
De Silva, G. M., Freeman, K. C., Bland-Hawthorn, J., et al. 2015, MNRAS, 449, 2604
Deepak, & Reddy, B. E. 2019, MNRAS, 484, 2000
Deheuvels, S., & Belkacem, K. 2018, A&A, 620, A43
Demarque, P., & Mengel, J. G. 1971, ApJ, 164, 317
Gaia Collaboration, Brown, A. G. A., Vallenari, A., et al. 2018, A&A, 616, A1
Gaia Collaboration, Prusti, T., de Bruijne, J. H. J., et al. 2016, A&A, 595, A1
Herwig, F., Bloecker, T., Schoenberner, D., & El Eid, M. 1997, A&A, 324, L81
Kjeldsen, H., & Bedding, T. R. 1995, A&A, 293, 87
Knauth, D. C., Federman, S. R., & Lambert, D. L. 2003, ApJ, 586, 268
Kumar, Y. B., Reddy, B. E., Campbell, S. W., et al. 2020, NatAs, 4, 1059
Kumar, Y. B., Reddy, B. E., & Lambert, D. L. 2011, ApJL, 730, L12
Lind, K., Asplund, M., & Barklem, P. S. 2009, A&A, 503, 541
Liu, C., Fu, J., Shi, J., et al. 2020, arXiv:2005.07210
Mocák, M., Siess, L., & Müller, E. 2011, A&A, 533, A53
Mori, K., Kusakabe, M., Balantekin, A. B., Kajino, T., & Famiano, M. A. 2021, MNRAS, 503, 2746
Mosser, B., Benomar, O., Belkacem, K., et al. 2014, A&A, 572, L5
Mosser, B., Goupil, M. J., Belkacem, K., et al. 2012a, A&A, 540, A143
Mosser, B., Goupil, M. J., Belkacem, K., et al. 2012b, A&A, 540, A143
Paxton, B., Bildsten, L., Dotter, A., et al. 2011, ApJS, 192, 3
Paxton, B., Smolec, R., Schwab, J., et al. 2019, ApJS, 243, 10
Reimers, D. 1975, Problems in Stellar Atmospheres and Envelopes (New York: Springer-Verlag), 229
Schwab, J. 2020, ApJL, 901, L18
Schwarzschild, M., & Härm, R. 1962, ApJ, 136, 158
Silva Aguirre, V., Ruchti, G. R., Hekker, S., et al. 2014, ApJL, 784, L16
Singh, R., Reddy, B. E., Bharat Kumar, Y., & Antia, H. M. 2019, ApJL, 878, L21
Smiljanic, R., Franciosini, E., Bragaglia, A., et al. 2018, arXiv:1805.07077
Sneden, C. A. 1973, PhD thesis, Univ. Texas
Sweigart, A. V. 1994, ApJ, 426, 612
Takeda, Y., & Tajitsu, A. 2017, PASJ, 69, 74
Thomas, H. C. 1967, ZAp, 67, 420
Torres, G. 2010, AJ, 140, 1158
Unno, W., Osaki, Y., Ando, H., Saio, H., & Shibahashi, H. 1989, Nonradial Oscillations of Stars (2nd ed.; Tokyo: Univ. Tokyo Press)
Vrard, M., Mosser, B., & Samadi, R. 2016, A&A, 588, A87
Wallerstein, G., & Sneden, C. 1982, ApJ, 255, 577
Yan, H.-L., Zhou, Y.-T., Zhang, X., et al. 2021, NatAs, 5, 86
Yu, J., Huber, D., Bedding, T. R., et al. 2018, ApJS, 236, 42